Palaeontology The Palaeontological Association www.palass.org

[Palaeontology, 2023, e12649]

Potential of closed contour analysis for species differentiation and holotype designation: a case study on lower Norian (Upper Triassic) conodonts

by ATTILA VIRÁG[1,2,3]* *and* VIKTOR KARÁDI[4]

[1]Department of Mineralogy & Geology, Institute of Earth Sciences, University of Debrecen, 1 Egyetem tér, Debrecen, H-4032, Hungary; virag.attila@science.unideb.hu, attila.virag@ttk.elte.hu

[2]Department of Petrology & Geochemistry, Institute of Geography & Earth Sciences, Eötvös Loránd University, 1/c Pázmány Péter sétány, Budapest, H-1117, Hungary

[3]MTA-MTM-ELTE Research Group for Paleontology, Hungary, 1/c Pázmány Péter sétány, Budapest, H-1117, Hungary

[4]Department of Palaeontology, Institute of Geography & Earth Sciences, Eötvös Loránd University, 1/c Pázmány Péter sétány, Budapest, H-1117, Hungary; karadi.viktor@ttk.elte.hu

*Corresponding author

Typescript received 9 September 2022; accepted in revised form 2 March 2023

Abstract: Geometric morphometric approaches become increasingly applied in the fields of biology and palaeontology. Taxonomy is a good example, where a long-standing intention of scientists is to eliminate subjectivity as much as possible. In the case of biostratigraphically important conodont elements, the application of such methods is not widespread. Only a handful of studies attempted to deal with the morphological variance of conodont elements from this aspect. The detailed description of five lower Norian (Upper Triassic) taxa (*Ancyrogondolella quadrata*, *A. rigoi*, *A. triangularis*, *A. uniformis* and *Metapolygnathus mazzai*) is presented here based on landmarks and Fourier analysis of the P_1 element and keel outlines. Both methods led to similar outcomes regarding taxonomic differentiation and exposing shape variability. Consensus shapes were generated to objectively reveal the typical contour shape of each taxon, which allowed their comparison with each other, and with the members of their respective sample population including the holotypes. The results demonstrated that the holotype of a taxon is generally not an average representative, but rather a peripheral form with well separable morphological characteristics. *Ancyrogondolella quadrata* and *A. rigoi* turned out to represent a morphological continuum with ample transitional forms between these two end-members that may cause bias in their biostratigraphic applicability, however their combined shape variance seems to be too large for uniting them into a single species. Given the results that may be too subtle to realize based solely on qualitative observations, future taxonomic studies and type material designation could greatly benefit from the application of similar methodologies.

Key words: conodont, Upper Triassic, landmark analysis, Fourier analysis, principal component analysis, consensus shape.

CONODONT animals were members of an extinct class of eel-like jawless vertebrates (Donoghue *et al.* 2000), ranging from the mid-Cambrian to the latest Triassic or earliest Jurassic (Sweet 1988; Kozur & Mock 1991; Du *et al.* 2020). Apart from some very special cases when the imprint of the whole animal is preserved (e.g. Briggs *et al.* 1983), the fossil remains are generally represented by conodont elements (marked with letters M, S and P), the phosphatic tooth-like structures of the bilaterally symmetrical feeding apparatus of the animal. Rarely, the entire apparatus of an individual can be found on bedding planes (natural assemblages), or some of the elements with physical contact fuse together diagenetically (fused clusters). Most often, however, the apparatus collapses after the death of the animal and the conodont elements fossilize isolated. In many cases, especially in the Triassic where natural assemblages are extremely rare, it is unknown which elements of the different types belonged to the same individual. Consequently, single elements with different morphologies are described as separate species with separate holotype elements. These are practically morphospecies and not species in the biological sense. This taxonomical concept is not unique in palaeontology as it is also common practice in palaeobotany (Taylor *et al.* 2009).

The information on the palaeobiology of the conodont animal that is lost through taphonomy has negligible effect on the geological application of conodont elements. Their abundance, rapid evolution and high resistance to diagenetic alteration (e.g. Epstein *et al.* 1977; Trotter &

doi: 10.1111/pala.12649

Eggins 2006) and their high preservation potential in tectonically deformed rocks (e.g. Sudar & Kovács 2006) make them one of the most widely used microfossils in applied geosciences. There are examples of the use of conodont elements in hydrocarbon exploration (e.g. Perry *et al.* 1983), ore exploration (e.g. Goebel 1996), mapping of hotspot tracks (e.g. Crough 1981), and geodynamics and basin evolution (e.g. Gawlick *et al.* 1994). Although these fields are of great importance too, conodont elements apparently have their primary role in biostratigraphy and the relative dating of marine rocks, predominantly of basin facies. P_1 elements in particular (Fig. 1) exhibit extensive and obvious morphological change (e.g. absence or presence of a platform, platform shape, platform length relative to the element length, denticle shape and abundance, shape of keel) during the evolution of the group. An accurate biostratigraphical application can only be based on a thorough and steady taxonomical framework. Primarily, taxa diagnoses are based on qualitative criteria. However, the subjective definition of the morphological features induces differing taxonomical concepts among individual researchers that may cause biases in stratigraphic subdivision (for discussion see Mazza *et al.* 2018). Such issues can be improved by studying the intra- and interspecific variability of species using objective and easily applicable geometric morphometric (GM) methods.

During the last few decades, landmark (LM) and Fourier descriptor (FD) based techniques have been used more and more frequently to provide quantitative support for qualitative interpretations on the morphological variation and apparent shape evolution of conodont elements. While landmark-based approaches allow the association of statistical variation with particular features on the studied morphology, Fourier analysis provides the most accurate representation of outlines, but it does not keep track of any particular points or incorporate meaningful information within the outline.

Jones *et al.* (2009) experimented with different techniques based on traditional measurements, landmarks and Fourier descriptors to differentiate the morphologically similar P_1 and P_2 elements of the Silurian *Wurmiella excavata*. They concluded that while in some individuals these elements are distinct from one another, in others they are practically indistinguishable. Suttner *et al.* (2017) used landmark analysis to aid the description of a new Middle Devonian conodont P_1 element, *Icriodus marieae*. Hogancamp & Manship (2016) tried several different approaches on the platform elements of the Late Devonian genus *Palmatolepis* to decide which techniques are the most appropriate for discriminating species. They found that landmark analysis was more effective in the separation of the taxa than other methods based on elliptical Fourier descriptors or linear measurements extracted from landmark coordinates. However, they also noted, that due to the morphological variety of the P_1 elements of different conodont species, it is likely that different techniques will vary in their utility for particular groups. Girard & Renaud (2011), as a critique of Klapper & Foster (1986, 1993) showed that while discriminant analysis based only on unambiguously determined individuals was able to clearly differentiate four *Palmatolepis* P_1 element species, a principal component analysis that included specimens with more dubious taxonomy resulted in a more realistic morphospace that showed continuous transitions between the end-members.

Renaud & Girard (1999) applied Fourier analysis on P_1 elements of Late Devonian *Icriodus* and *Palmatolepis* and discovered that their size and shape changes inversely throughout the studied section. They explained this phenomenon with environmental changes caused by the Kellwasser crisis. Through a similar Fourier analysis Girard & Renaud (2008) revealed that allometry is the major source of shape variation in the case of the P_1 elements of the Late Devonian *Ancyrodella*. Using a multivariate regression approach, they separated this size-related variation from the size-free shape changes and concluded that the reason for the extinction of this genus cannot be attributed to an absence of a morphological response to the Kellwasser event. Renaud *et al.* (2020) applied a landmark-based methodology to quantify the shape of Late Devonian *Polygnathus* P_1 elements. They compared the 2D and 3D approaches and validated a 2D description as an efficient approximation of the 3D geometry. Their 3D analysis delivered insights into the relationship between the geometry of the elements and the constraints related to occlusion, whereas the 2D analysis allowed a quantitative assessment of the variation among species and through time. They also demonstrated that extensive intraspecific variation largely obliterated taxonomic and temporal differences in their sample population. Renaud *et al.* (2021) studied the shape variation of *Palmatolepis* P_1 elements during the Late Devonian by the means of a Fourier analysis. They hypothesized that the morphology changed due to environmental fluctuations impacting the faunas by moving adaptive optima and thus selecting for new mean shapes and new types of variants around the mean shape. They found that the mean shape was conserved during periods of relatively stable environmental conditions, but was shifted from broad elements with a large platform to slender elements devoid of platform. They explained the latter phenomenon as a response to environmental oscillations culminating in the Frasnian–Famennian mass extinction (i.e. the Kellwasser event).

Hogancamp *et al.* (2016) used a landmark-based approach with eigen analyses to reveal the shape variation within P_1 elements of the Late Carboniferous *Idiognathodus simulator* group and concluded that it comprises a set of at least five species. Zimmermann *et al.* (2018) performed landmark analysis on P_1 elements of seven Late

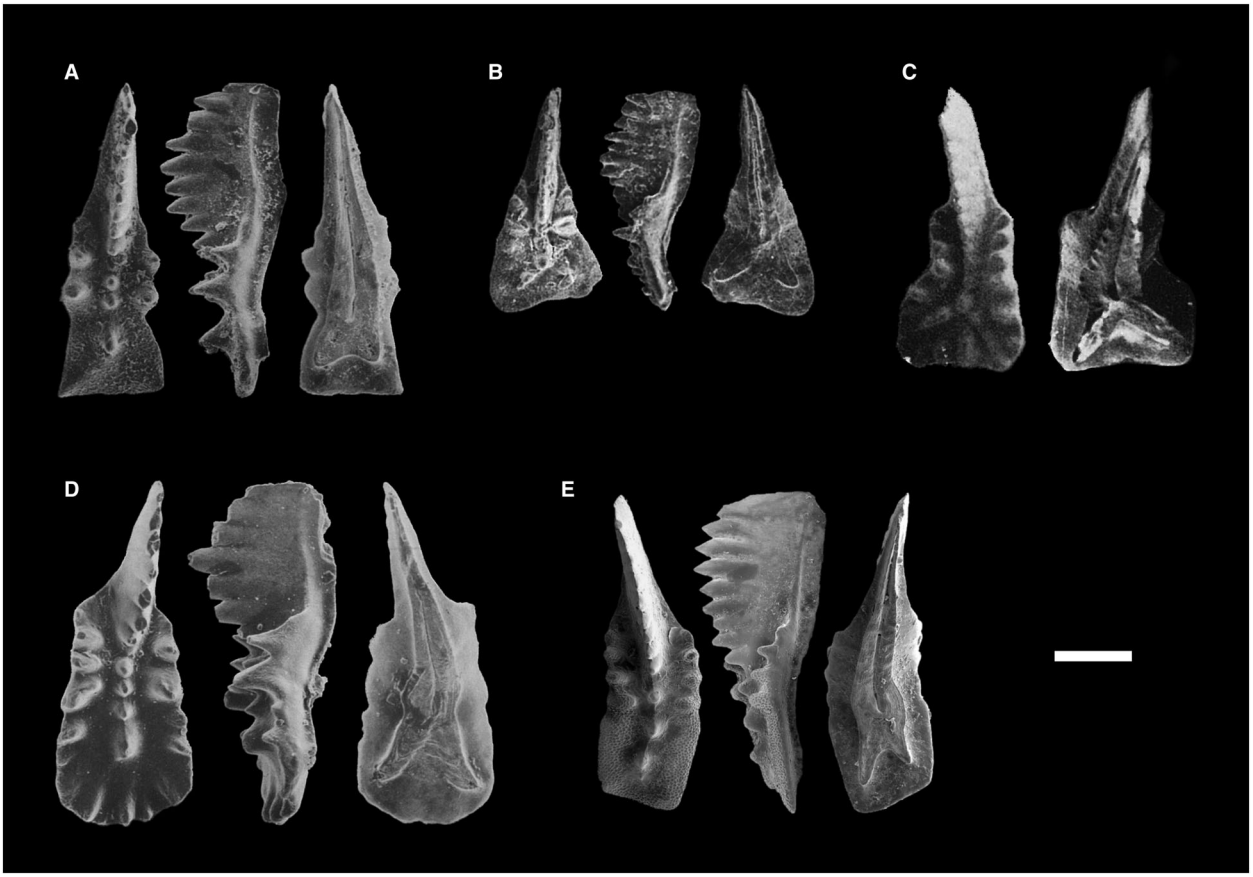

FIG. 1. The holotype specimens of the studied P_1 element species. All shown in oral, lateral and aboral view, respectively, unless otherwise stated. A, *Ancyrogondolella quadrata* from Pardonet Hill, northeastern British Columbia, Canada (GSC 95265; re-figured from Orchard 1991, pl. 2, figs 1–3). B, *Ancyrogondolella rigoi* from Stefanion, Greece (UPMC L157; re-figured from Noyan & Vrielynck 2000, fig. 8.4). C, *Ancyrogondolella triangularis* from Kälberstein, Germany (GIBAS 2103/1; re-figured from Budurov 1977, pl. 5, figs 20, 21); oral and aboral views only. D, *Ancyrogondolella uniformis* from Pardonet Hill, northeastern British Columbia, Canada (GSC 95272; re-figured from Orchard 1991, pl. 3, figs 1–3). E, *Metapolygnathus mazzai* from Pizzo Mondello, Sicily, Italy (MPUM FNP134; re-figured from Mazza *et al.* 2012*a*, pl. 8, fig. 12). *Repository abbreviations*: GIBAS, Geological Institute of the Bulgarian Academy of Sciences; GSC, Geological Survey of Canada; MPUM FNP, Museum of Paleontology, University of Milan, Facies Nereo Preto; UPMC Pierre and Marie Curie University, Paris. Scale bar represents 200 μm.

Carboniferous *Neognathodus* species but recognized only five different morphotypes within their sample population. Based on their findings, they synonymized two pairs of statistically indistinguishable species. They also studied the patterns of morphological change throughout time and defined four distinct biozones, which coincided with previously published schemes.

Despite the fact that similar issues are also relevant to Triassic conodont research, apparently fewer studies have focused on this period. Chen *et al.* (2016) investigated the P_1 elements of the Anisian (Middle Triassic) *Paragondolella* via landmark analysis. They recognized a linear relationship between the shape and size of *P. bifurcata*. Because of this allometric growth pattern, they suggested that the taxonomic classification of platform conodonts and the definition of new species should be based on large and ontogenetically older specimens. Landmark analysis was combined recently with more traditional (angle and linear distance) measurements on aboral and lateral views of P_1 elements (including the holotypes) of the Olenekian (Early Triassic) *Neospathodus* by Guenser *et al.* (2022). They tested the effect of the sample size on the observed morphological variability of a group and taxonomic determination. They discovered that their methodology was able to detect four morphospecies when less than 20% of the specimens in a larger assemblage were considered, whereas it recognized only two forms when at least 30% of their total sample population were included in the analysis. Without further discussion, they also made the assumption that the intraspecific variation does not necessarily distribute symmetrically around the holotype. They suggested that future works should be

based not only on the unambiguously determined specimens but also on those transitional forms that are hardly assignable to established species. They encouraged researchers to extensively illustrate, measure and quantitatively describe morphological variability in their material to better constrain delineation of taxa.

Guenser *et al.* (2019) used a landmark-based approach combined with elliptical Fourier analysis of the aboral margin and the element outline in oral view in order to study intra- and interspecific variation of seven Late Triassic conodont morphospecies (including their holotypes) of the Carnian–Norian boundary interval. They revealed a parallel evolutionary path for the *Carnepigondolella–Metapolygnathus* and *Carnepigondolella–Epigondolella* lineages. This observation was based on a common pattern of intraspecific and intergeneric morphological variation, probably due to intrinsic, developmental constraints. They also observed that the morphological transition between Carnian forms and their presumed Norian descendants followed a trajectory that was different from this line of least resistance, suggesting that strong extrinsic pressures, such as environmental disturbances, were probably at play during this interval, and the evolution of these elements might reflect adaptations to new diets. Four holotypes (*Carnepigondolella zoae*, *C. pseudodiebeli*, *Metapolygnathus communisti* and *Epigondolella rigoi*) fell within the range of variation of their respective sample populations but the holotypes of the other three studied species (*Hayashiella tuvalica*, *E. quadrata* and *E. uniformis*) did not. It has to be noted though, that the holotype of *M. communisti* is situated in a peripheral position within the corresponding convex hull of the species. A rather recent article by Souquet *et al.* (2022), that was published after the first version of the current paper was submitted, used a landmark-based approach to quantify the morphology of P_1 elements (including holotypes) deriving from two different time periods: the Devonian–Carboniferous boundary and the Late Triassic Carnian–Norian boundary. For this latter interval, they used exactly the same species from the same section as Guenser *et al.* (2019). Souquet *et al.* (2022) arrived at a similar conclusion in the case of both intervals as Guenser *et al.* (2019) and assumed that the observed morphological evolution was driven by environmental perturbations related to changes in ocean temperature. Regarding the holotype specimens, without marking their exact position in their principal component analysis based morphospace, they noted that all fell within the respective 95% concentration ellipses of their corresponding sample populations. They also mentioned that excluding these specimens from the analysis slightly affected the explanatory power of the principal component axes.

The present study focuses on early Norian (Late Triassic) conodont P_1 elements, an assemblage younger than those of the above cited studies, although slightly overlapping with the time interval investigated by Guenser *et al.* (2019) and Souquet *et al.* (2022). Norian biostratigraphy is hampered by several taxonomical issues that mainly derive from the overly general original diagnoses and/or the sparse illustration of the species characteristic for this age (Karádi 2018*a*). Descriptions of species rarely include detailed comparison with other taxa from the same time interval (e.g. Budurov 1972), therefore many specimens with potentially transitional characters either fit in more than one species or do not fully fit in any established species, which results in taxonomic and stratigraphic ambiguities. The aim of this study is to test whether objective geometric morphometric methodologies can reveal such morphological relationships that are, at first glance, not so obvious when working with conodont elements solely from a qualitative point of view, and thus improve taxonomic subdivisions. The research is based on the comparison of outline quantification gained from landmark and Fourier descriptor analyses, as in Hogancamp & Manship (2016) but on markedly different morphologies and from a different time interval. By mathematically producing mean P_1 element shapes for the studied species, we aim to anchor the analysis of intra- and interspecific variability to an objective basis. This has importance in examining whether the original descriptions are strict enough for the secure identification of specimens. Additionally, we compare the holotypes with the general shape of their respective species and their respective sample population, which has not previously been attempted on conodonts in such detail.

MATERIAL AND METHOD

The analysis involved a total of 136 lower Norian conodont P_1 elements (Table 1) that can be considered an average size statistical sample in the Triassic in comparison with the studies by Guenser *et al.* (2019, 2022) and Souquet *et al.* (2022). The material originates from various localities of the western Tethys and western North America. Tethyan specimens are from the Dovško section in Slovenia (Karádi *et al.* 2021), the Csővár area and the Buda Hills in Hungary (Karádi *et al.* 2016; Karádi 2018*b*), the Pizzo Mondello section in Italy (Mazza *et al.* 2012*a*), the Kälberstein quarry in Germany (Budurov 1972) and the Stefanion section in Greece (Noyan & Kozur 2007). North American conodonts are from Pardonet Hill, Childerhose Cove and Carbon Creek east in Canada (Orchard 1991, 2018). Conodonts from Dovško, Csővár and the Buda Hills were chosen from the material of previous stratigraphic research and mapping campaigns, during which approximately 3 kg of rock was processed per sample. These rock samples represent point samples in certain cases, when the outcrop at a locality exposed only a few beds and not a thick sedimentary

TABLE 1. List of the studied material with specific determination, number of specimens, and reference for the image of holotype that was digitized.

Taxon	Number of specimens	Reference for image of holotype
Ancyrogondolella quadrata	35	Orchard (1991)
Ancyrogondolella ex gr. *quadrata*	12	–
Ancyrogondolella rigoi	42	Noyan & Vrielynck (2000)
Ancyrogondolella ex gr. *rigoi*	8	–
Ancyrogondolella triangularis	15	Budurov (1977)
Ancyrogondolella uniformis	12	Orchard (1991)
Ancyrogondolella ex gr. *uniformis*	2	–
Metapolygnathus mazzai	6	Mazza *et al.* (2012*a*)
Metapolygnathus ex gr. *mazzai*	4	–

sequence. Specimens from the Dovško section are stored in the collections of the Geological Survey of Slovenia (Ljubljana) and specimens from the Csővár area and the Buda Hills are housed in the Department of Palaeontology at the Eötvös Loránd University (Budapest, Hungary). For the rest of the localities, images were digitized from the plates of Mazza & Martínez-Pérez (2015), Mazza *et al.* (2012*a*), Nicora *et al.* (2007), Noyan & Kozur (2007) and Orchard (1991, 2018).

Of the specimens considered, 80% were unambiguously assigned to the taxa *Ancyrogondolella quadrata*, *A. rigoi*, *A. triangularis*, *A. uniformis* and *Metapolygnathus mazzai*. For specimens bearing morphological characters not fully fitting the original diagnoses of these species, the open nomenclatural term '*ex gr.*' (of the group) was used. Holotypes of the listed species were also included in the study based on best illustrations from the literature (the used depictions of *A. rigoi*, *A. triangularis* and *M. mazzai* were taken from publications that do not contain their original descriptions).

Only undeformed, complete, adult (GS4–GS6; based on the ontogenetic series defined in Mazza & Martínez-Pérez 2015) specimens were involved in the present study. The P_1 elements were sputter-coated with gold palladium and photographed in oral and aboral views partly by a Hitachi S-2600N scanning electron microscope at the Department of Botany of the Hungarian Natural History Museum (Budapest), and a JEOL IT500HR scanning electron microscope at the Szentágothai Research Centre of the University of Pécs. See additional information on each specimen in Virág & Karádi (2023).

Taxonomic notes

The comparison of the (P_1 element) species (*Ancyrogondolella quadrata*, *A. rigoi*, *A. triangularis*, *A. uniformis* and *Metapolygnathus mazzai*) included in the present study is difficult if based only on the original diagnoses, since those are often very brief and incomplete, and different authors had different ideas about the important morphological characters when establishing a species. Nowadays, conodont specialists use a more or less uniform system with well-defined traits to describe new species, and give detailed diagnoses and comprehensive comparisons with other taxa. In this section, a list and concise explanations of the key morphological features are given, which are considered in the descriptions and determinations of most Upper Triassic P_1 conodont species. In a broader sense these can be applied for the entire Triassic. Table 2 shows an extract of the original diagnoses of the five studies species in the light of the recently used morphological characters. The original diagnosis of *A. uniformis* is rather problematic, because Orchard (1991) first described it as a subspecies of *A. triangularis* and, as such, the detailed description and the comparison with other taxa were given under *A. triangularis* without clear distinction of what refers to *A. uniformis*. The holotypes of the study's P_1 conodont species are shown in Figure 1. The key morphological traits of Upper Triassic P_1 conodont species are as follows.

Platform shape. The outline of the platform in oral and aboral views. It can be extremely variable with several transitional options between triangular, rectangular, ovoid, circular and posteriorly pointed. Visible in the oral and aboral outlines of the element.

Free blade length. The part of the blade that is not bordered by the platform on either side (Fig. 2A, B). If the platform covers the entire length of the element, no free blade is present. Visible in the oral and aboral outlines of the element. See Mazza *et al.* (2012*b*, fig. 2).

Anterior trough margin. The anteriormost part of the platform in oral view, just anterior to the first denticle of the anterior platform margins, where the platform meets the blade. If it is well-developed, the platform connects the blade gradually. If it is reduced, the platform connects the blade abruptly. Visible in the oral and aboral outlines of the element. See Figure 2B and Mazza *et al.* (2012*b*, fig. 2).

Platform margin denticulation. The presence of nodes or denticles on the margins of the platform in oral view (Fig. 2B). Not visible in the keel and element outlines.

TABLE 2. An extract of the original diagnoses of the five studied species in the light of the key morphological characters used in recent literature.

Taxon	*A. quadrata*	*A. rigoi*	*A. triangularis*	*A. uniformis*	*M. mazzai*
Reference	Orchard 1991	Noyan & Kozur 2007	Budurov 1972	Orchard 1991	Karádi *et al.* 2013
Platform shape	Rectangular	Subtriangular	*Ancyrognathus*-like, broad	Subrectangular	Rectangular
Free blade length	Up to 1/2 unit length	Not specified	Not specified	Not specified	1/2 unit length
Anterior trough margin	Not specified	Not specified	Not specified	Not specified	Not specified
Platform margin denticulation	Few denticles on the anterior margins	2–4 denticles on the anterior margins	Denticles on all margins	Denticles on all margins	2–5 nodes or short denticles on the anterior margins
Posterior carina	Not specified	1 denticle; secondary posterior carina may develop	Secondary posterior carina	Not specified	2–3 large nodes
Pit position	Central	Central	Not specified	Subcentral	Central or slightly forward-shifted
Keel termination	Bifurcated	Bifurcated	Bifurcated	Bifurcated	Irregularly bifurcated
Lateral profile	Arched	Not specified	Not specified	Arched	Not specified

A., *Ancyrogondolella*; *M.*, *Metapolygnathus*.

Posterior carina. The presence of carinal nodes or denticles posterior to the cusp in oral view. It also defines the position of the cusp. Secondary posterior carina may develop towards the posterolateral corners of the platform. Not visible in the keel and element outlines. See Karádi (2021, figs 1, 4) for examples.

Pit position. The location of the pit within the platform in aboral view (Fig. 2C). It can be situated in the mid-length of the platform, in the anterior half (forward shifted) or in the posterior half of the platform (where it can be terminal or sub-terminal). Not visible in the keel and element outlines.

Keel termination. The shape of the posterior end of the keel in aboral view (Fig. 2C). It can be pointed, rounded, blunt or bifurcated. It can show asymmetry. Visible in the keel outline.

Lateral profile. The line of the lower margin in lateral view. It can be arched, stepped, straight and upturned. Visible in the lateral outline of the element. See Figure 2A and Karádi (2021, fig. 3) for examples.

Landmark analysis

For the shape description we chose to analyse the element and the keel outlines, which contain important characters (e.g. general shape, anterior platform termination, keel termination). Since only closed contours or open but continuous segments are accessible for Fourier analysis, we also focused on these features for the landmark analysis, to allow the comparison of results. We minimized the number of LMs that are not lying on the contours, however, we retained the position of the cusp and the pit, as their locations are key diagnostic traits in every P_1 element (Sweet 1988). The latter contour was not considered in the present study because of inconsistencies in the orientation of SEM photos in the literature, which cause distortion and prevent comparison. See the differences between the slightly oblique view in Mazza *et al.* (2012*a*) and the exact lateral view in Orchard (1991). To avoid bias induced by bilaterality, all dextral elements (*sensu* Purnell *et al.* 2000) were mirrored into their sinistral counterpart, since Guenser *et al.* (2019) pointed out that there is no significant shape difference between the original and mirrored P_1 elements of conodonts comparable in both age and morphology with the species studied here. Similar conclusions were drawn by Renaud & Girard (1999) and Girard & Renaud (2008) regarding the symmetry of the platform elements of Late Devonian genera *Ancyrodella*, *Icriodus* and *Palmatolepis*.

Outline digitization was carried out manually (as in Sinitsa *et al.* 2019) using the multi-point tool of the open access ImageJ software (v1.53; Abramoff *et al.* 2004; Schneider *et al.* 2012). Uniform point allocation was achieved by the equidistantCurve function of the Morpho package within the R programming environment (v4.1.2; R Core Team 2013; Schlager 2017). In total, the

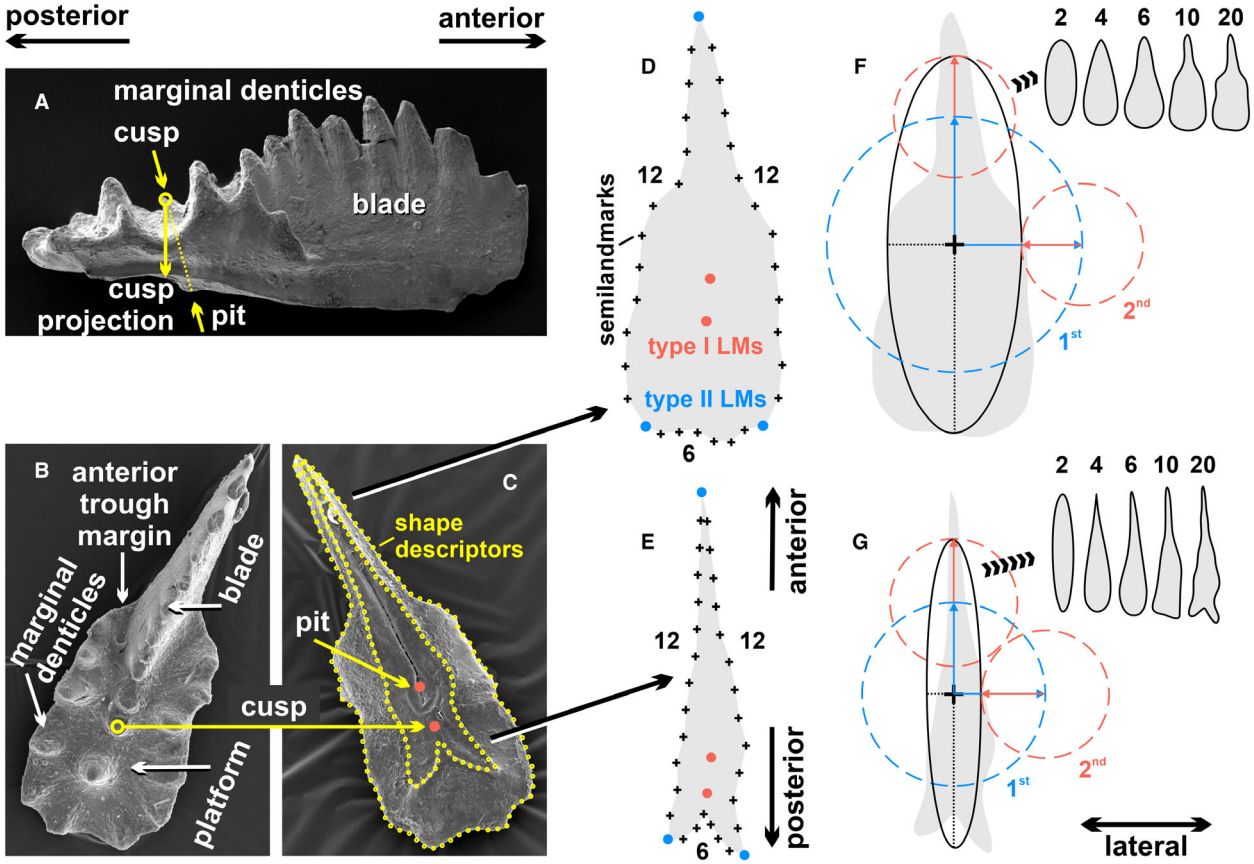

FIG. 2. A–C, *Ancyrogondolella uniformis* P_1 element from the Csővár borehole (Csv-1, Hungary; ELTE 410–149), with anatomical terms and directions used herein, and the 100 equidistantly placed shape descriptors of the keel and element outlines (C); in: A, lateral; B, oral; C, aboral view. D–E, type II landmarks (LMs) were identified via a computer-aided approach, and the contour sections between them were resampled by a pre-defined number of semilandmarks. F–G, via the superimposition of epicycles resulting from the forward complex discrete Fourier transformation (DFT) of the shape descriptors, the original contours can be smoothed to a desired degree; the more epicycles are used, the better the approximation will be; see text for further explanation. *Repository abbreviation*: ELTE, Eötvös Loránd University, Budapest.

coordinates of 100 shape descriptors (yellow circles in Fig. 2C) were recorded to describe the element and keel outlines, separately. In addition, the position of the pit was marked in aboral view. To be able to record the position of the tip of the cusp, which is not visible in this view, images made in oral view were mirrored and projected onto the corresponding aboral views (Fig. 2B, C). The more posteriorly inclined the cusp, the further behind the pit its projection falls (Fig. 2A). The digitized contours are available in Virág & Karádi (2023).

The points related to the location of the cusp and the pit were recognized as type I landmarks (i.e. homologous anatomical points; orange filled circles in Fig. 2C–E). Type II or geometrical landmarks (*sensu* Bookstein 1992; blue filled circles in Fig. 2D, E) were selected on the outlines using automated algorithms that searched for the sharpest inward facing angle between neighbouring equidistant shape descriptors of a specific region. On the element outline, the anterior end and the posterolateral corners were marked. On the keel outline, the anterior end and the two posterior tips (if the keel was bifid) or the posterolateral corners (if the keel was non-bifid; e.g. in some specimens of *A. uniformis*) were selected. The sections between the type II landmarks were resampled by a pre-defined number of equidistantly placed non-sliding semilandmarks (6 on the posterior margin and 12 on each lateral margins; black crosses in Fig. 2D, E) to record finer details of the shape (see Gunz & Mitteroecker 2013). The number of semilandmarks was chosen so that the points have a similar density on both the lateral and the posterior margins in the case of most studied specimens. However, the constraints of the LM analysis require the placement of equal numbers of points on identical segments. Thus, if the length of a specific segment changes (e.g. due to variations in the extent of keel bifurcation), it can result in unequal densities for some outlines.

To eliminate variability induced by size and orientational differences, a generalized Procrustes superimposition was used; the LM configurations (Fig. 2D, E) were centred, scaled to the same centroid size, and rotated until the minimum sum of squared distances between the LMs and their corresponding average position was reached (Gower 1975). To extract the primary patterns of variation, a principal component analysis (PCA) was performed on the resulting aligned coordinates with the prcomp function of the built-in stats package in R. The aligned LM configurations and the resulting PCA scores are provided in Virág & Karádi (2023).

Fourier analysis

Using forward complex discrete Fourier transformation (DFT), any closed contour defined by a set of 2D coordinates can be decomposed to a sum of circular motions with harmonic frequencies called epicycles or rotating phasors (Kuhl & Giardina 1982; Haines & Crampton 2000; Smith 2002; Godefroy *et al.* 2012). The number of the resulting epicycles is identical with the number of the points in the original outline. The characteristics of each epicycle (i.e. its amplitude and starting phase angle) are defined by two coefficients often referred as Fourier descriptors (FDs). These FDs were calculated here using equation 31.6 of Smith (2002) and a custom function (dft; Virág & Karádi 2023) written in R programming language (v4.1.2; R Core Team 2013). The previously produced coordinate sets containing 100 equidistant shape descriptors (visible in Fig. 2C) were used as the basis for these calculations; thus the DFT resulted in 100 pairs of FDs for each analysed outline. Contrary to the LM-based approach, the positions of the pit and the cusp were ignored, and all contour points (including the ones selected before as type II LMs) were treated equally during the Fourier analysis. The amplitude and phase of an epicycle was determined by substituting its FDs into equation 8.6 of Smith (2002). An initial outline can be synthesized via superimposing the resulting epicycles in a decreasing order of amplitude (where each new one is centred around the endpoint of the previous phasor). The first two epicycles (defined by four FDs) describe an ellipse that loosely approximates the general shape. By the addition of more epicycles, the produced contour will gradually converge towards the actual outline (Fig. 2F, G). Consequently, this inverse DFT approach (implemented using R function invDft; Virág & Karádi 2023) allows the smoothing of contours with varying degrees by summing only the first epicycles.

In order to use FDs for the purpose of contour comparison, they must be made independent of the size and the orientation of the original outline, as well as the starting point of the last phasor on the contour. This normalization both in 2D and 3D typically uses the above mentioned first ellipse as a reference (see in Fig. 2F, G). Following the steps described by Kuhl & Giardina (1982) and Godefroy *et al.* (2012), the FDs were rescaled here so that the major axis of the first ellipse (i.e. the sum of the amplitudes of the first two epicycles) became equal to 1. The centred outlines were rotated until the minor and major axes coincided with the horizontal and vertical axes of the underlying Cartesian coordinate system. The FDs were also corrected so that the starting phase angle of the first two epicycles became 0. These steps were achieved by a specifically designed R function (normDft; Virág & Karádi 2023). As with the LM configurations, the resulting Fourier coefficients were used as variables in a PCA implemented by the prcomp function of the built-in stats package of R. Only the first 20 pairs of FDs were considered for this analysis to provide a good balance between a satisfying description of the element shape, and an efficient filtering of measurement noise without using excessive epicycles. The normalized FDs and the resulting PCA scores are provided in Virág & Karádi (2023).

Consensus shapes

Both Procrustes fitted landmark configurations and contour points resulting from an inverse DFT using the same number of epicycles can form the basis of a calculation that produces the consensus shape of a specific group. One only needs to average the positions of all corresponding points within the group in order to synthesize a mean outline that represents the typical appearance of the underlying sample population. However, it is important to keep in mind that none of the existing specimens in the sample used for the calculation necessarily has the exact same contour as their consensus. In a PCA morphospace, the consensus shape is located at the centroid of the group on which is was based (Gower 1975). To be able to objectively describe and compare the general outline characteristics of the studied groups, consensus shapes were generated here for all P_1 elements together (grey shaded silhouettes in Fig. 3), and for each species separately (black contours in Fig. 4). Specimens with uncertain taxonomic identifications were excluded from the species level consensus shape calculations.

RESULTS

PCA-based shape spaces

The first two axes of the LM-based PCA explain together more than 50% of the total variance both for the element and keel outlines (Fig. 3A, B) in aboral view. Groups are best

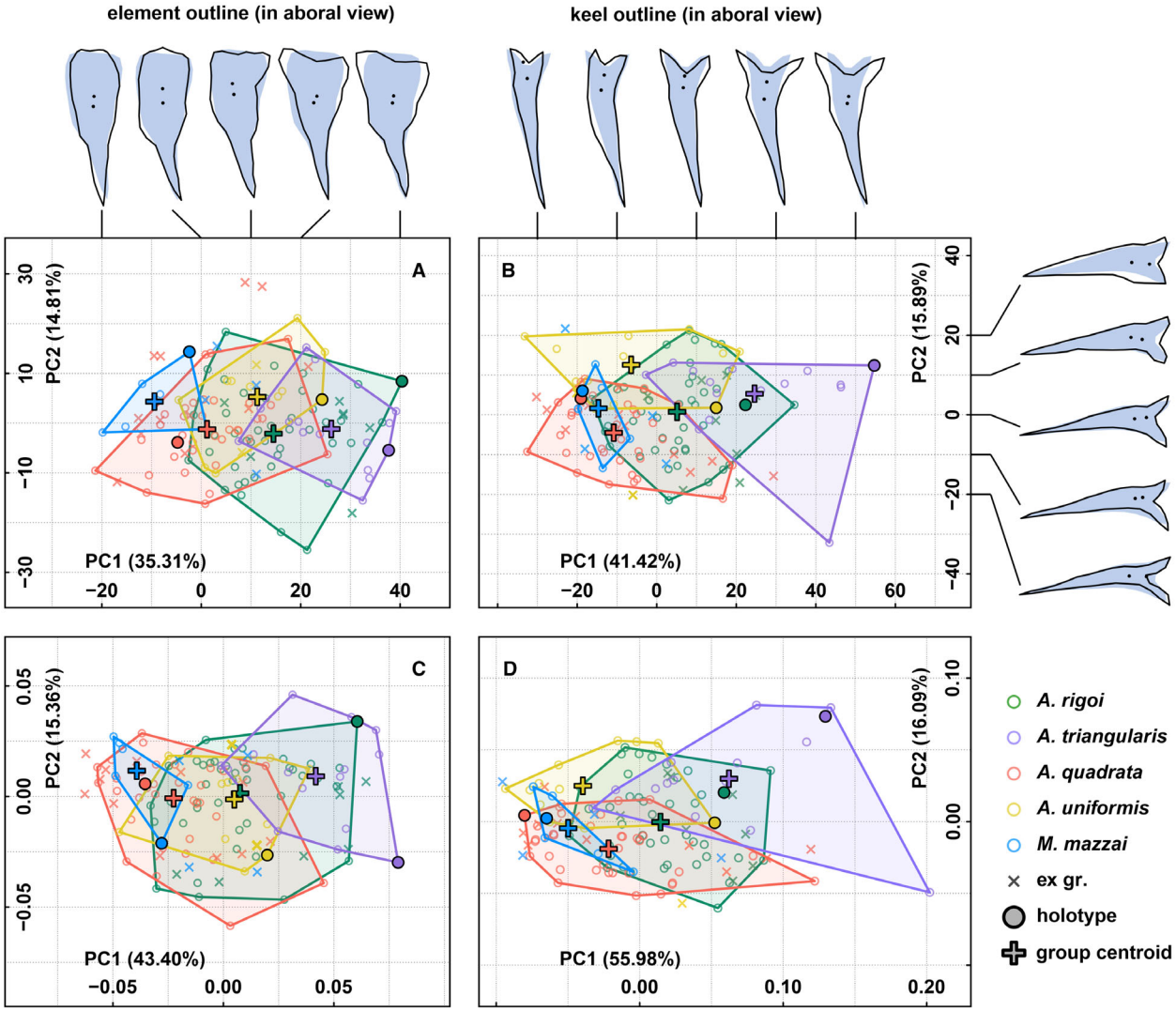

FIG. 3. A–B, the first two axes of the principal component analysis (PCA) of the landmark configurations. C–D, the first 20 pairs of Fourier descriptors. Shape changes along the axes are shown for the element outline on A and for the keel on B by black contours. The grey shaded silhouettes represent the consensus morphology for all studied specimens.

separated by the PCA based on the keel outline (Fig. 3B). *Ancyrogondolella quadrata* (orange), *A. triangularis* (purple) and *A. uniformis* (yellow) have only minimal overlap with each other within the morphospace. *Ancyrogondolella rigoi* (green) has a central position, partially overlapping with all groups. *Metapolygnathus mazzai* (blue) is intermediate between *A. quadrata* and *A. uniformis*, but clearly distinct from *A. triangularis*, being located on the opposite end of the first principal component (PC1). The groups have larger overlaps within the morphospace generated by the PCA of the element outline (Fig. 3A) compared to the keel outline (Fig. 3B).

The arrangement of the species in the morphospace generated by the PCA of the first 20 pairs of FDs (Fig. 3C, D) shows great similarity with the outcome described above. It is important to emphasize that each FD-based PCA ordination of our data display basically the same group structure if it includes at least the first four coefficient pairs. If only these four pairs are used, just the immensely smoothed representations of the contours (as visible in Fig. 2F, G) are compared. By raising the number of the FDs used, the discrimination barely improves. This means that the general differences of the outlines are mainly responsible for the visible grouping, and the finer details of the contours are not as influential.

Since the outcomes of the landmark and Fourier descriptor based approaches are considerably similar, the

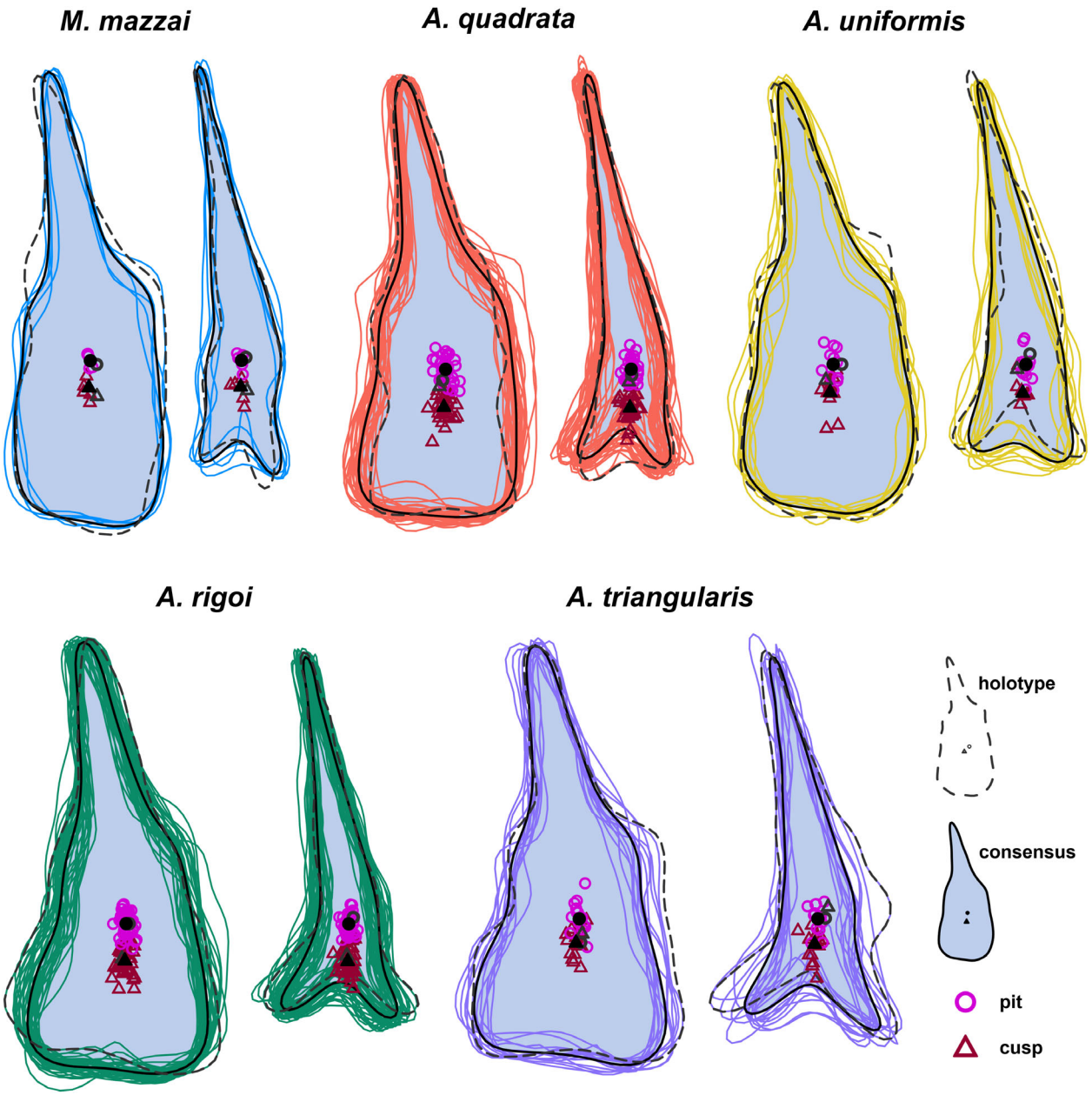

FIG. 4. Mathematically produced consensus shapes of the analysed species (black contours) projected over the outlines of other specimens assigned to the respective groups. The contours were smoothed using an inverse DFT approach based on their first 20 epicycles. Holotypes are highlighted with dashed lines. Pit locations are marked by circles, whereas cusp projections are indicated by triangles (both shapes are filled in the case of the consensus configurations).

shape changes assignable to the principal components are only illustrated for the LM-based outcome (Fig. 3A, B), and are not presented separately for the FD-based ordination. Along the first axis, the element outline changes from a shape characterized by subparallel margins (*M. mazzai*) to a posterolaterally more extended, subtriangular to triangular contour (*A. triangularis*). In the same direction, the posterior platform margin transforms from straight to slightly concave (Fig. 3A). Along the second axis, no remarkable outline shape change can be observed. Following the posterior widening of the platform, the posterolateral lobes of the keel also extend visibly along PC1 in Figure 3B. The second principal component displays a change in the extent of keel bifurcation from a strongly bifid outline with long posterior lobes (*A. quadrata*) to a slightly bifid one with short lobes (*A. uniformis*). Interestingly, the more extended the bifurcation, the narrower the keel is.

Consensus shapes

The mathematically-produced consensus configurations of the analysed species (Fig. 4) are the objective representations of their general shapes, which can be described as follows:

1. *Metapolygnathus mazzai* is slender, having a rectangular platform with subparallel margins. The anterior platform termination is abrupt. The pit is located clearly anterior to the mid-length of the platform. The keel shows a moderate posterior bifurcation that develops relatively far behind the pit.
2. *Ancyrogondolella quadrata* is characterized by a rectangular platform with posteriorly slightly diverging margins and a gradual anterior platform termination. The pit is situated at the mid-length of the platform. The keel is moderately bifid.
3. *Ancyrogondolella uniformis* has a subrectangular outline with posteriorly slightly expanding platform and rounded posterolateral corners. The anterior platform termination is gradual. The pit can be found at the mid-length of the platform. The projection of the cusp is not far behind the pit. The keel shows a modest posterior bifurcation.
4. *Ancyrogondolella rigoi* has a wedge-shaped appearance with posteriorly markedly diverging platform margins. The anterior platform termination is barely demarcated, which makes the determination of pit position complicated, but it seems to be located slightly in front of the platform mid-length. The keel has a moderate posterior bifurcation with outward oriented lobes.
5. *Ancyrogondolella triangularis* is characterized by a triangular shape with the anterior platform termination being gradual. The pit is situated at the mid-length of the platform. The projection of the cusp is close to the position of the pit. The keel is moderately bifid and its lobes point outward.

Holotypes in the morphospace

Based on the PCA of the element outlines, the holotype of *M. mazzai* (blue circle with black border in Fig. 3A) is distinct from the other groups. Although the sample number is small, it is located in a peripheral position of the current convex hull, relatively far from the group centroid (blue cross in Fig. 3A). Its difference from the consensus shape is expressed by the markedly longer platform in relation to the element length and the slightly more asymmetric appearance (Fig. 4). Considering the PCA-based analysis of the keel outlines (Fig. 3B) it is located much closer to the group centroid; however, it plots over the convex hulls of both *A. quadrata* (orange) and *A. uniformis* (yellow). Compared to the consensus shape and the rest of the specimens, even its keel bifurcation is more asymmetric (Fig. 4).

Regarding its element outline, is the holotype of *A. quadrata* located close to the group centroid (orange cross in Fig. 3A), despite the pronounced constriction at the mid-length of the platform, which is lacking on the consensus shape and not typical for the rest of the specimens in such an extent (Fig. 4). Concerning the keel contour, it has a peripheral position (Fig. 3B). Differing from the majority of *A. quadrata* specimens, the keel end is only weekly bifurcated, and thus, it shows a moderate prolongation behind the pit (Fig. 4). This may also explain why this specimen is close to the holotype of *M. mazzai*.

In the PCA based on the element outlines (Fig. 3A), the holotype of *A. uniformis* is located at the positive end of the convex hull, closer to the centroid of *A. triangularis* (purple cross) than to that of its own group (yellow cross). Its platform length compared to the element length is the longest among the studied specimens of the same taxon (Fig. 4). It plots over the convex hulls of both *A. rigoi* (green) and *A. triangularis* (purple). Likewise, it has a peripheral position on the PCA based on the keel outline (Fig. 3B). It is situated closer to the centroids of both *A. rigoi* (green cross) and *A. triangularis* (purple cross) than to that of its own group (yellow cross), and it plots close to the holotype of *A. rigoi*. The posterior keel end has a strongly bifid appearance compared to the consensus shape and the rest of the specimens (Fig. 4).

Along the horizontal axis of Figure 3A, the holotype of *A. rigoi* is located on the positive end of the entire sample population, since this specimen has one of the posteriorly most widened platforms, even wider than most elements assigned to *A. triangularis*. Correspondingly, the spread of its keel lobes is also extremely wide (Fig. 4). Consequently, it is located close to the centroid of *A. triangularis* (purple cross in Fig. 3B). It also plots close to the holotype of *A. uniformis* with a similar PC2 value on Figure 3B, despite the evident differences in their keel contours.

The holotype of *A. triangularis* is clearly distinct from the other groups, as it is in a peripheral position, near the positive end of the first axis in regard of both the element and keel outlines (Fig. 3A, B). It is similar to the holotype of *A. rigoi* in the aspect of the broadness of the posterior part of the platform, consequently, they are relatively close to each other in Figure 3A. Compared to the rest of the specimens in its own group, the greatest difference is expressed in the keel contour. The bulge at the level of the pit is the most pronounced in the holotype, and also the spread of its keel lobes is extreme (Fig. 4).

DISCUSSION

Intraspecific variance

Compared to the above described consensus shapes, each group has a natural shape variability (Fig. 4), which is caused by several factors. One of them is ontogeny, resulting in minor variations of the morphological characters, even between adult growth stages (i.e. GS4–GS6). Such a difference is evident in the development of the anterior trough margin, which affects the relative length of the platform. Compare for example the *Ancyrogondolella rigoi* specimens illustrated by Mazza *et al.* (2012*a*, pl. 6, figs 1–7). Another bias is caused by gradual evolutionary trends that can happen in short timespans and affect not only intrageneric lineages (Orchard 1983; Karádi 2021) but even a single species. Such examples can be seen in the descriptions of the Carnian–Norian boundary species *Kraussodontus peteri*, *Quadralella deflecta* and *Q. posteroexpansa* provided by Orchard (2014), who used the platform length versus blade length ratio, the element size and carina length, and variance in the pit position to distinguish stratigraphically older and younger morphotypes within the species.

In an ideal case, these sources of morphological noise should be eliminated by selecting specimens from only one growth stage and a single, well constrained time horizon. This would mean the investigation of single beds of successions representing a high sedimentation rate (i.e. not condensed). To gain sufficiently large numbers of specimens, the dissolution of excessive rock samples (tens of kg) would be necessary, which is acid-consuming and often limited by available laboratory space. A further issue would be to find the exactly contemporaneous time horizon in another section. But even if it was possible, the problem of ecomorphotypical variance would still remain. Realistically, these conditions cannot be achieved. Therefore, one must be aware of inevitable distortion during the evaluation of the results of such analyses. One should keep in mind that the following interpretations might be biased by the fact that the studied specimens originate from various levels of the early Norian (spanning approximately 2–3 million years; Gehrels *et al.* 1987; Diakow *et al.* 2012; Kent *et al.* 2017).

In the case of *Metapolygnathus mazzai*, the intraspecific variation is most expressed in the platform length relative to the element length, although this species was represented by the lowest number of specimens. High deviation can also be observed in the extent of the keel bifurcation. Unlike in *M. mazzai*, platform length relative to the element length seems more consistent in *Ancyrogondolella quadrata*. A few specimens are characterized by greater width of the anterior platform that results in a more abrupt anterior termination of the platform in these cases compared to the majority of the element outlines. The posterior keel termination is moderately to strongly bifid, apart from a few outliers. The extent of the outward orientation of the lobes varies greatly, but in general, the lobes are more diverging than in *M. mazzai*.

The platform length relative to the element length seems also consistent in *A. uniformis*, however, few specimens differ from the majority in this regard. Interestingly, these specimens are also characterized by an abrupt anterior platform termination that is not common in the group. Independent of the platform length, its posterior part is always slightly wider than its anterior part. The extent of the keel bifurcation shows a great variability from almost non-bifid to moderately bifid, even strongly bifid in one case.

The overall element outline shape seems consistent in *A. rigoi*, however, there is a notable deviation of the platform width. A few specimens stand out from the group by having a notch in the middle of the posterior platform margin. The keel bifurcation shows great variance with all possible morphologies from an almost blunt to a strongly bifid termination. A slight change is visible in the spread of its lobes: the broader the platform, the wider their spread is.

In the case of *A. triangularis*, the platform length relative to the element length varies depending on how developed the anterior trough margin is, which also defines the shape of the anterior platform termination. The width of the posterior part of the platform is not strictly dependent of the width of the anterior part, which results in specimens with a sudden narrowing between the posterior and anterior part of the platform. There is a variation in the shape of the posterior platform margin from straight to slightly concave appearance. The largest deviation of the keel contour can be observed in *A. triangularis*. The extent of the keel bifurcation varies from moderately to strongly bifid, and likewise in *A. rigoi*, the orientation of its lobes is influenced by the width of the posterior part of the platform. A typical trait in most of the *A. triangularis* specimens is a distinct bulge on one side of the keel contour at the level of the pit.

Interspecific variance

In order to reveal interspecific differences, it is important to evaluate where the groups (or specific individuals within them) are located in the PCA-based morphospaces (Fig. 3) and how high the degree of their separation is. The further apart two groups are located, and the smaller their intersection is, the fewer similarities the species share and the fewer transitional forms exist. However, one should keep in mind, that Figure 3 is the result of

dimensionality reduction, during which several original variables with decreasing importance were inherently reduced. Thus, the Euclidean distances of the points in these projections only approximate their true distances in the multidimensional space of all original variables.

Based on the PCA of the element outlines (Fig. 3A) *M. mazzai* (blue), *A. uniformis* (yellow) *and A. triangularis* (purple) form relatively distinct clouds in the morphospace differentiated from each other by the increasingly diverging lateral platform margins. The partial overlap of *M. mazzai* with *A. uniformis* does not hamper the distinction of the two taxa, since they clearly differ in their marginal denticulation and posterior carina, mentioned in their original diagnoses. Note that these characters are not included in the present outline analysis, because denticulation falls in the area inside the outline. The partial overlap of *A. uniformis* and *A. triangularis* is rather problematic, because it shows that posteriorly more expanded *A. uniformis* specimens and posteriorly less expanded *A. triangularis* specimens also exist. In addition, the holotype of *A. uniformis* is situated closer to the centroid of *A. triangularis* than to that of its own group. According to the original diagnosis of *A. uniformis* (Orchard, 1991), it can be distinguished from *A. triangularis* by the less expanded posterior platform and the weaker marginal denticulation. However, posteriorly more expanded specimens with weak marginal denticulation are also known from the fossil record, as well as posteriorly less expanded specimens with strong denticulation (e.g. Karádi *et al.* 2021, fig. 6(5–7)). This demonstrates that the original diagnoses are not sufficient to distinguish these P_1 conodont morphospecies in all cases, which emphasizes the importance of objectively revealing intraspecific variance within larger assemblages in the future.

Ancyrogondolella quadrata (orange) overlaps mainly with *M. mazzai* and *A. uniformis*, with only one point plotting deeply in the *A. triangularis* sample population. Specimens in the *A. quadrata* sample population exist both with parallel and sub-parallel lateral platform margins, which explains the partial overlap of the orange cloud with the blue and yellow groups. For the same reason, *A. rigoi* (green), that can have posteriorly slightly or strongly expanded platform, overlaps with the subrectangular *A. uniformis* and the triangular *A. triangularis*. The distinction of *A. rigoi* from the latter two taxa can be reliably based on the platform margin denticulation, since *A. uniformis* and *A. triangularis* have denticles all over the platform margins (Budurov 1972; Orchard 1991; Mazza *et al.* 2012*a*), whereas the lateral and posterior platform margins are smooth in *A. rigoi* (Noyan & Kozur 2007; Mazza *et al.* 2012*a*).

A large part of the *A. rigoi* sample population shares common space with *A. quadrata*, too. This intersection contains the posteriorly narrower *A. rigoi* specimens and the posteriorly broader *A. quadrata* specimens. Since *A. quadrata* is also characterized by undenticulated lateral and posterior platform margins (Orchard 1991; Mazza *et al.* 2012*a*), the element outline is considered to be an important trait in the distinction of the two species. But the results of our analysis revealed a continuous morphological series with all transitions present between a rectangular specimen of *A. quadrata* and a subtriangular specimen of *A. rigoi*. This is the same issue as between *A. uniformis* and *A. triangularis* discussed above. Figure 3 shows that it is not only the ambiguously determined individuals that are responsible for this transition, nor are these *ex gr.* specimens restricted to the intersecting area of the two species.

Similar morphological continuities seem to occur frequently among coeval conodont morphospecies, since Guenser *et al.* (2022) discussed a comparable situation in Lower Triassic, platformless P_1 *Neospathodus* spp. elements. What makes it more important is the fact that these latter Lower Triassic taxa have markedly different characteristics from the Upper Triassic elements studied in this paper, since they have no platform and no keel. The analyses of Guenser *et al.* (2022) were based on the lateral element outline and the contour of the lower margin, where all key morphological characters of the neospathids are visible. The Upper Triassic platform-bearing elements of our study, however, have important traits that fall within the outlines and thus cannot be included in the present shape analyses. These morphological features will need to be quantified and combined with the morphometric analyses of the outlines, but this is clearly out of the scope of the present research. A future study could investigate whether such an approach would result in a better delineation of taxa, and might also help to better understand the relations of the *ex gr.* specimens with more clearly established morphologies.

The results based on the keel outlines (Fig. 3B) show that *A. quadrata* and *A. uniformis* are clearly distinct from one another along PC2, even though there is a narrow intersection of their convex hulls. Generally, *A. quadrata* is characterized by a strongly bifid and narrow keel, whereas most of the specimens assigned to *A. uniformis* have a broader keel with weaker bifurcation. However, the situation is somewhat more complex. Although, the extent of keel bifurcation and the overall width of the keel usually correlate with each other (i.e. wider keels tend to be less bifid and vice versa), they can change independently to some extent. The position of specimens with a similar rate of bifurcation along PC2 is defined solely by the overall width of the keel: the broader the keel, the greater the PC2 value. Likewise, greater PC2 values characterize the position of specimens with similar keel widths, but weaker bifurcation. The simultaneous

change of each trait results in two shifts along the vertical axis that can have the same or opposing signs. In the former case, the specimen will definitely move in one direction along the second axis. However, in the latter case, if the extent of the opposing shifts is the same, the effects can negate each other, causing no movement at all. Consequently, two specimens with different keel widths can be situated at the same PC2 value on Figure 3B if this difference is compensated by the extent of their keel bifurcation. Such a situation is demonstrated, for example by the holotypes of *A. quadrata* and *A. uniformis*, where the former has a narrow but weakly bifid keel, and the latter has a broad but strongly bifid keel. The same is true for the holotype of *A. quadrata* when compared to the holotype of *A. rigoi* (Fig. 4). The holotype of *A. quadrata* is evidently an extreme specimen regarding its keel outline, what may also explain why it is so close to the holotype of *M. mazzai* (Fig. 3B), which also has a posteriorly prolonged, weakly bifid keel (Fig. 4).

Regarding the extent of keel bifurcation and the overall width of the keel (Fig. 3B), *A. triangularis* represents a transitional morphology between *A. quadrata* and *A. uniformis* apart from one outlier that has a strongly bifid keel contour. The wider spread of its keel lobes results in a partial separation from both groups, since many specimens are shifted towards a more positive direction along the first axis. Considering all aspects of the keel shape, its convex hull still has an intersection with that of *A. uniformis*. Similarly, *M. mazzai* occupies an intermediate position between *A. quadrata* and *A. uniformis* along the second axis. However, the narrow spread of its keel lobes places the sample population towards the negative end of the horizontal axis, close to the opposing side of the used morphospace relative *A. triangularis*. Specimens with a more strongly bifid keel may be similar to *A. quadrata*, but other morphological traits (i.e. more than one denticle in the posterior carina behind the cusp, Karádi *et al.* 2013), not visible in the present outline analysis, secure the distinction of *M. mazzai*.

The keel characteristics of *A. rigoi* place the group in a central position within the morphospace (Fig. 3B). Regarding the spread of its keel lobes, the horizontal axis is characterized by the lack of extreme end-members. Considering the overall width and the extent of keel bifurcation, *A. rigoi* has all possible morphological options that occur in the other taxa. Consequently, its convex hull has notable overlaps with all studied groups. As noted above, if one considers traits that are not related to the element or keel contour (e.g. platform denticulation or posterior carinal denticles), *A. uniformis*, *A. triangularis* and *M. mazzai* can easily be distinguished from *A. rigoi*. However, there is a problem with *A. quadrata*, with which *A. rigoi* also shares a common space based on the keel morphology. It can be stated that there is no sharp division between the two taxa due to the considerable number of transitional forms. Hence, in this case, closed contour analysis cannot aid the taxonomist to reduce subjectivity. Using synchrotron x-ray tomography, Mazza & Martínez-Pérez (2015) discovered that the posterior carinal denticle is already present in the earliest growth stage (GS1) in *A. rigoi*, but only develops in a later growth stage (usually GS4) in *A. quadrata*. Even if it is a novel discovery, it does not help the differentiation of adult specimens without using a synchrotron. Moreover the frequent application of such an equipment is too expensive to be realistic for species determination in stratigraphic practice.

Concerning the holotypes of the studied P_1 conodont morphospecies, the results of our research strongly suggest that taxonomists often choose specimens with clearly distinct morphologies that often represent end-members in an assemblage. This is not surprising in the light of the existence of many specimens with transitional characters towards other species with similar appearance (as in the case of *A. rigoi* and *A. quadrata*), where diagnostic traits are hard to catch. The present study pointed out that the typical representative of a sample population can be objectively selected by the application of equivalent geometric morphometric approaches (e.g. Hogencamp & Manship 2016; Suttner *et al.* 2017), which we recommend should be considered in the future for the designation of the type material of a new taxon.

CONCLUSION

The results of the present paper prove that both the landmark and Fourier descriptor based geometric morphometric approaches were able to distinguish P_1 elements of different conodont morphotaxa based on their aboral outline and keel contour, leading to essentially identical outcomes. This observation supports the conclusions of Hogancamp & Manship (2016).

The geometric morphometric analysis highlighted that the outlines of certain, currently used conodont morphospecies (e.g. *Ancyrogondolella quadrata* and *A. rigoi*) vary on a great range with a plethora of transitional morphologies that hinders their secure distinction. Although the merging of such groups seems plausible, in fact it is still impractical, since their combined shape variance might be unrealistically large compared to the more separable coexisting forms. Moreover, it may hamper the biostratigraphic applicability assuming that the end-members of the morphoseries do not have exactly the same stratigraphic ranges. We believe that in stratigraphic practice, without a thorough taxonomic revision, it is better to use open nomenclature rather than assigning the individuals

to specific taxa if an assemblage contains only specimens with ambiguous characteristics.

In assemblages where interspecific morphological continuity is not present to such an extent, generating a consensus shape by similar geometric morphometric approaches can reveal the typical characteristics of the sample population. This should be considered in the description of new species and the designation of their holotypes in order to avoid the selection of extreme forms as type material, as seen in the case of the investigated lower Norian taxa. Morphological variance (i.e. individual points within a morphospace) should be distributed more or less evenly around the type specimen, if possible. This helps to prevent our understanding shifting away from the morphological variance expressed in the original assemblage when additional material is recovered. In the species diagnoses, more emphasis should be placed on the intraspecific variability exposed by objective shape analysing methods.

Coupling the outline characteristics presented herein with the analysis of independent data (e.g. to describe the platform denticulation or the number of posterior carinal denticles) might improve taxonomic differentiation in the future. Beside coeval assemblages, the analytical procedure applied herein might also help to establish objective boundaries within evolutionary lineages. The comparison of assemblages of remote palaeogeographic regions (e.g. western Tethys, eastern Tethys and eastern Panthalassa in the Triassic) would also benefit from a similar contour analysis by revealing whether endemism or contrasting taxonomical concepts are responsible for their assumed faunal differences.

Acknowledgements. We are grateful to the reviewers of this paper, Pauline Guenser and Emilia Jarochowska, for their useful and constructive comments. The authors are indebted to Krisztina Buczkó and to Péter Szabó for their help in taking scanning electron micrographs. Thanks are due to Tea Kolar-Jurkovšek from the Geological Survey of Slovenia for her invaluable contribution in the stratigraphic project of the Dovško section, the material of which is included in this study. The ample free online material created by Daniel Shiffman aided writing the functions used here for the Fourier transformation. Financial support was provided to AV from the NKFIH FK 128741 project and to VK from the Arthur James Boucout Research Grant of the Paleontological Society. The staff of the Department of Palaeontology of the Eötvös Loránd University is also acknowledged.

Author contributions. VK identified the conodont elements, made the scanning electron micrographs and digitized the element and keel outlines. AV wrote the R scripts, analysed the data and prepared the figures. Both authors took equal part in evaluating the results of the analyses and writing the original draft of the manuscript.

DATA ARCHIVING STATEMENT

Data for this study, including detailed information on each studied conodont P_1 element, the digitized element and keel contours, the landmark configurations and the Fourier descriptors of each outline, the results of the principal component analyses, and two R scripts containing all used custom functions and examples for the method of their application are available in the Dryad Digital Repository: https://doi.org/10.5061/dryad.g1jwstqv9

Editor. Paul Smith

REFERENCES

ABRAMOFF, M. D., MAGALHAES, P. J. and RAM, S. J. 2004. Image processing with ImageJ. *Biophotonics International*, **11**, 36–42.

BOOKSTEIN, F. 1992. *Morphometric tools for landmark data: Geometry and biology*. Cambridge University Press, 435 pp.

BRIGGS, D. E. G., CLARKSON, E. N. K. and ALDRIDGE, R. J. 1983. The conodont animal. *Lethaia*, **16**, 1–14.

BUDUROV, K. J. 1972. *Ancyrogondolella triangularis* gen. et sp. n. (Conodonta). *Mitteilungen der Gesellschaft der Geologie- und Bergbaustudenten*, **21**, 853–860.

BUDUROV, K. J. 1977. Revision of the Late Triassic platform conodonts. *Geologica Balcanica*, **7**, 31–48.

CHEN, Y., NEUBAUER, T. A., KRYSTYN, L. and RICHOZ, S. 2016. Allometry in Anisian (Middle Triassic) segminiplanate conodonts and its implications for conodont taxonomy. *Palaeontology*, **59**, 725–741.

CROUGH, S. T. 1981. Mesozoic hotspot epeirogeny in eastern North America. *Geology*, **9**, 2–6.

DIAKOW, L., ORCHARD, M. J. and FRIEDMAN, R. 2012. Absolute ages for the Norian Stage: a further contribution from southern British Columbia, Canada. Cordilleran Tectonics Workshop, Geological Association of Canada, Pacific Section, 2.

DONOGHUE, P. C., FOREY, P. L. and ALDRIDGE, R. J. 2000. Conodont affinity and chordate phylogeny. *Biological Reviews*, **75**, 191–251.

DU, Y., CHIARI, M., KARÁDI, V., NICORA, A., ONOUE, T., PÁLFY, J., ROGHI, G., TOMIMATSU, Y. and RIGO, M. 2020. The asynchronous disappearance of conodonts: new constraints from Triassic-Jurassic boundary sections in the Tethys and Panthalassa. *Earth-Science Reviews*, **203**, 103176.

EPSTEIN, A. G., EPSTEIN, J. B. and HARRIS, L. D. 1977. Conodont color alteration – an index to organic metamorphism. *Geological Survey Professional Paper*, **995**, 1–27.

GAWLICK, H. J., KRYSTYN, L. and LEIN, R. 1994. Conodont colour alteration indices: palaeotemperatures and metamorphism in the Northern Calcareous Alps — a general view. *Geologische Rundschau*, **83**, 660–664.

GEHRELS, G. E., SALEEBY, J. B. and BERG, H. C. 1987. Geology of Annette, Gravina, and Duke islands, southeastern Alaska. *Canadian Journal of Earth Sciences*, **24**, 866–881.

GIRARD, C. and RENAUD, S. 2008. Disentangling allometry and response to Kellwasser anoxic events in the Late Devonian conodont genus *Ancyrodella*. *Lethaia*, **41**, 383–394.

GIRARD, C. and RENAUD, S. 2011. The species concept in a long-extinct fossil group, the conodonts. *Comptes Rendus Palevol*, **10**, 107–115.

GODEFROY, J. E., BORNERT, F., GROS, C. I. and CONSTANTINESCO, A. 2012. Elliptical Fourier descriptors for contours in three dimensions: a new tool for morphometrical analysis in biology. *Comptes Rendus Biologies*, **335**, 205–213.

GOEBEL, E. D. 1996. The pathway for MVT hydrothermal fluids within the Tri-state mining district from stratigraphic plotting of conodont alteration indices. 413–418. *In* SANGSTER, D. F. (ed.) *Carbonate-hosted lead-zinc deposits*, **4**. Society of Economic Geologists, Special Publication.

GOWER, J. C. 1975. Generalized Procrustes analysis. *Psychometrika*, **40**, 33–51.

GUENSER, P., SOUQUET, L., DOLÉDEC, S., MAZZA, M., RIGO, M. and GOUDEMAND, N. 2019. Deciphering the roles of environment and development in the evolution of a Late Triassic assemblage of conodont elements. *Paleobiology*, **45**, 440–457.

GUENSER, P., GINOT, S., ESCARGUEL, G. and GOUDEMAND, N. 2022. When less is more and more is less: the impact of sampling effort on species delineation. *Palaeontology*, **65**, e12598.

GUNZ, P. and MITTEROECKER, P. 2013. Semilandmarks: a method for quantifying curves and surfaces. *Hystrix*, **24**, 103–109.

HAINES, A. J. and CRAMPTON, J. S. 2000. Improvements to the method of Fourier shape analysis as applied in morphometric studies. *Palaeontology*, **43**, 765–783.

HOGANCAMP, N. J. and MANSHIP, L. L. 2016. Comparison of morphometric techniques and the ability to accurately reconstruct the form and distinguish between species of the *Palmatolepis winchelli* group – Conodonta, Upper Devonian. *Micropaleontology*, **62**, 439–451.

HOGANCAMP, N. J., BARRICK, J. E. and STRAUSS, R. E. 2016. Geometric morphometric analysis and taxonomic revision of the Gzhelian (Late Pennsylvanian) conodont *Idiognathodus simulator* from North America. *Acta Palaeontologica Polonica*, **61**, 477–502.

JONES, D., PURNELL, M. A. and VON BITTER, P. H. 2009. Morphological criteria for recognising homology in isolated skeletal elements: comparison of traditional and morphometric approaches in conodonts. *Palaeontology*, **52**, 1243–1256.

KARÁDI, V. 2018*a*. Middle Norian conodonts from the Buda Hills, Hungary: an exceptional record from the Western Tethys. *Journal of Iberian Geology*, **44**, 155–174.

KARÁDI, V. 2018*b*. Triassic conodonts from the Csővár area and the Buda Hills, Hungary and their geological applications. PhD thesis, Department of Palaeontology, Eötvös Loránd University, Budapest, 120 pp.

KARÁDI, V. 2021. Evolutionary trends of the genus *Ancyrogondolella* (Conodonta) and related taxa in the Norian (Late Triassic). *Journal of Earth Science*, **32**, 700–708.

KARÁDI, V., KOZUR, H. W. and GÖRÖG, Á. 2013. Stratigraphically important Lower Norian from the Csővár borehole (Csv-1), Hungary – comparison with the conodont succession of the Norian GSSP candidate Pizzo Mondello (Sicily, Italy). *New Mexico Museum of Natural History & Science Bulletin*, **61**, 284–295.

KARÁDI, V., PELIKÁN, P. and HAAS, J. 2016. Conodont biostratigraphy of Upper Triassic dolomites of the Buda Hills (Transdanubian Range, Hungary). *Bulletin of the Hungarian Geological Society*, **146**, 371–386.

KARÁDI, V., KOLAR-JURKOVŠEK, T., GALE, L. and JURKOVŠEK, B. 2021. New advances in biostratigraphy of the lower/middle Norian transition: Conodonts of the Dovško Section, Slovenia. *Journal of Earth Science*, **32**, 677–699.

KENT, D. V., OLSEN, P. E. and MUTTONI, G. 2017. Astrochronostratigraphic polarity time scale (APTS) for the Late Triassic and Early Jurassic from continental sediments and correlation with standard marine stages. *Earth-Science Reviews*, **166**, 153–180.

KLAPPER, G. and FOSTER, C. T. Jr 1986. Quantification of outlines in Frasnian (Upper Devonian) platform conodonts. *Canadian Journal of Earth Sciences*, **23**, 1214–1222.

KLAPPER, G. and FOSTER, C. T. Jr 1993. Shape analysis of Frasnian species of the Late Devonian conodont genus *Palmatolepis*. *The Paleontological Society Memoir*, **32**, 1–35.

KOZUR, H. and MOCK, R. 1991. New Middle Carnian and Rhaetian conodonts from Hungary and the Alps. Stratigraphic importance and tectonic implications for the Buda Mountains and adjacent areas. *Jahrbuch der Geologischen Bundesanstalt*, **134**, 271–297.

KUHL, F. P. and GIARDINA, C. R. 1982. Elliptic Fourier features of a closed contour. *Computer Graphics & Image Processing*, **18**, 236–258.

MAZZA, M. and MARTÍNEZ-PÉREZ, C. 2015. Unravelling conodont (Conodonta) ontogenetic processes in the Late Triassic through growth series reconstructions and X-ray microtomography. *Bollettino della Societa Paleontologica Italiana*, **54**, 161–186.

MAZZA, M., RIGO, M. and GULLO, M. 2012*a*. Taxonomy and biostratigraphic record of the Upper Triassic conodonts of the Pizzo Mondello section (western Sicily, Italy), GSSP candidate for the base of the Norian. *Rivista Italiana di Paleontologia e Stratigrafia*, **118**, 85–130.

MAZZA, M., CAU, R. and RIGO, M. 2012*b*. Application of numerical cladistic analyses to the Carnian–Norian conodonts: a new approach for phylogenetic interpretations. *Journal of Systematic Palaeontology*, **10**, 401–422.

MAZZA, M., NICORA, A. and RIGO, M. 2018. *Metapolygnathus parvus* Kozur, 1972 (Conodonta): a potential primary marker for the Norian GSSP (Upper Triassic). *Bollettino della Societa Paleontologica Italiana*, **57**, 81–101.

NICORA, A., BALINI, M., BELLANCA, A., BERTINELLI, A., BOWRING, S. A., DI STEFANO, P., DUMITRICA, P., GUAIUMI, C., GULLO, M., HUNGERBUEHLER, A., LEVERA, M., MAZZA, M., McROBERTS, C. A., MUTTONI, G., PRETO, N. and RIGO, M. 2007. The

Carnian/Norian boundary interval at Pizzo Mondello (Sicani Mountains, Sicily) and its bearing for the definition of the GSSP of the Norian Stage. *Albertiana*, **36**, 102–129.

NOYAN, Ö. F. and KOZUR, H. W. 2007. Revision of the late Carnian early Norian conodonts from the Stefanion section (Argolis, Greece) and their palaeobiogeographic implications. *Neues Jahrbuch für Geologie und Paläontologie (Abhandlungen)*, **245**, 159–178.

NOYAN, Ö. F. and VRIELYNCK, B. 2000. Importance of morphogenetic analysis in taxonomy: an example from Triassic platform conodonts. *Neues Jahrbuch für Geologie und Paläontologie Monatshefte*, **2000** (10), 577–594.

ORCHARD, M. J. 1983. *Epigondolella* populations and their phylogeny and zonation in the Upper Triassic. *Fossils & Strata*, **15**, 177–192.

ORCHARD, M. J. 1991. Upper Triassic conodont biochronology and new index species from the Canadian Cordillera. 299–335. *In* ORCHARD, M. J. and McCRACKEN, A. D. (eds) *Ordovician to triassic conodont paleontology of the Canadian Cordillera*, **417**. Bulletin of the Geological Survey of Canada.

ORCHARD, M. J. 2014. Conodonts from the Carnian-Norian boundary (Upper Triassic) of Black Bear Ridge, northeastern British Columbia, Canada. *New Mexico Museum of Natural History & Science Bulletin*, **64**, 1–139.

ORCHARD, M. J. 2018. The Lower-Middle Norian (Upper Triassic) boundary: new conodont taxa and a refined biozonation. *Bulletins of American Paleontology*, **395–396**, 165–193.

PERRY, W. J., WARDLAW, B. R., BOSTICK, N. H. and MAUGHAN, E. K. 1983. Structure, burial history, and petroleum potential of frontal thrust belt and adjacent foreland, southwest Montana. *AAPG Bulletin*, **67**, 725–743.

PURNELL, M. A., DONOGHUE, P. C. J. and ALDRIDGE, R. J. 2000. Orientation and anatomical notation in conodonts. *Journal of Paleontology*, **74**, 113–122.

R CORE TEAM. 2013. R: A language and environment for statistical computing. R Foundation for Statistical Computing, Vienna, Austria. https://www.R-project.org/

RENAUD, S. and GIRARD, C. 1999. Strategies of survival during extreme environmental perturbations: evolution of conodonts in response to the Kellwasser crisis (Upper Devonian). *Palaeogeography, Palaeoclimatology, Palaeoecology*, **146**, 19–32.

RENAUD, S., ECALLE, B., CLAISSE, P., CHARRUAULT, A., LEDEVIN, R. and GIRARD, C. 2020. Patterns of bilateral asymmetry and allometry in Late Devonian *Polygnathus* conodonts. *Palaeontology*, **64**, 37–159.

RENAUD, S., GIRARD, S. and DUFOUR, A.-B. 2021. Morphometric variance, evolutionary constraints and their change through time in Late Devonian *Palmatolepis* conodonts. *Evolution*, **75**, 2911–2929.

SCHLAGER, S. 2017. Morpho and Rvcg – shape analysis in R: R-packages for geometric morphometrics, shape analysis and surface manipulations. 217–256. *In* ZHENG, G., LI, S. and SZÉKELY, G. (eds) *Statistical shape and deformation analysis*. Academic Press, 488 pp.

SCHNEIDER, C. A., RASBAND, W. S. and ELICEIRI, K. W. 2012. NIH Image to ImageJ: 25 years of image analysis. *Nature Methods*, **9**, 671–675.

SINITSA, M. V., VIRÁG, A., PAZONYI, P. and KNITLOVÁ, M. 2019. Redescription and phylogenetic relationships of *Spermophilus citelloides* (Rodentia:Sciuridae: Xerinae), a ground squirrel from the Middle Pleistocene – Holocene of Central Europe. *Historical Biology*, **33**, 19–39.

SMITH, S. W. 2002. *Digital signal processing: A practical guide for engineers and scientists*. Elsevier, 650 pp.

SOUQUET, L., GUENSER, P., GIRARD, C., MAZZA, M., RIGO, M. and GOUDEMAND, N. 2022. Temperature-driven heterochrony as a main evolutionary response to climate changes in conodonts. *Proceedings of the Royal Society B*, **289**, 20220614.

SUDAR, M. and KOVÁCS, S. 2006. Metamorphosed and ductilely deformed conodonts from Triassic limestones situated beneath ophiolite complexes: Kopaonik Mountain (Serbia) and Bükk Mountains (NE Hungary) – a preliminary comparison. *Geologica Carpathica*, **57**, 157–176.

SUTTNER, T. J., KIDO, E. and SUTTNER, A. W. W. 2017. *Icriodus marieae*, a new icriodontid conodont species from the Middle Devonian. *Paläontologische Zeitschrift*, **91**, 137–144.

SWEET, W. C. 1988. *The Conodonta: morphology, taxonomy, paleoecology, and evolutionary history of a long-extinct animal phylum*. Oxford Monographs on Geology & Geophysics, 10, 224 pp.

TAYLOR, T. L., TAYLOR, E. L. and KRINGS, M. 2009. *Paleobotany: The biology and evolution of fossil plants*, Second edition. Elsevier, 1230 pp.

TROTTER, J. A. and EGGINS, S. M. 2006. Chemical systematics of conodont apatite determined by laser ablation ICPMS. *Chemical Geology*, **233**, 196–216.

VIRÁG, A. and KARÁDI, V. 2023. Data from: Potentials of closed contour analysis in species differentiation and holotype designation: a case study on lower Norian (Upper Triassic) conodonts. *Dryad Digital Repository*. https://doi.org/10.5061/dryad.g1jwstqv9

ZIMMERMANN, A. N., JOHNSON, C. C. and POLLY, P. D. 2018. Taxonomic and evolutionary pattern revisions resulting from geometric morphometric analysis of Pennsylvanian *Neognathodus* conodonts, Illinois Basin. *Paleobiology*, **44**, 660–683.